Available online at www.sciencedirect.com

SciVerse ScienceDirect

Ceramics International 38 (2012) 6613–6620

CERAMICS INTERNATIONAL

www.elsevier.com/locate/ceramint

Evaluation of hot corrosion behavior of plasma sprayed ceria and yttria stabilized zirconia thermal barrier coatings in the presence of $Na_2SO_4+V_2O_5$ molten salt

Raheleh Ahmadi-Pidani*, Reza Shoja-Razavi, Reza Mozafarinia, Hossein Jamali

Department of Materials Engineering, Malek-Ashtar University of Technology, Shahinshahr, Isfahan, Iran

Received 10 April 2012; received in revised form 14 May 2012; accepted 16 May 2012
Available online 23 May 2012

Abstract

In this study, substrates of Inconel 738 LC superalloy coupons were first sprayed with a NiCoCrAlY bondcoat and then with a ceria and yttria stabilized zirconia (CYSZ; ZrO_2-25 wt%$CeO_2-2.5$ wt%Y_2O_3) topcoat by air plasma spraying (APS). Hot corrosion studies of plasma sprayed thermal barrier coatings (TBCs) were conducted in 45 wt%Na_2SO_4+55 wt%V_2O_5 molten salt at 1000 °C for 30 h. The results showed that the coating defects, such as pores and microcracks play important roles as effective paths for the salt penetration in hot corrosion. Based on the results, the reaction between molten salt and stabilizers of zirconia (Y_2O_3 and CeO_2), the formation of YVO_4, $CeVO_4$ and CeO_2 crystals, the detrimental phase transformation of zirconia from tetragonal to monoclinic due to the depletion of stabilizers and finally, the creation of stresses were recognized to be in the degradation mechanism of CYSZ ceramic coatings in the presence of molten sulfate–vanadate salt.

Keywords: Thermal barrier coating; CYSZ; Air plasma spraying; Hot corrosion

1. Introduction

Thermal barrier coatings (TBCs) are used to provide thermal insulation to the hot section components of gas turbines in order to protect them from thermal degradation and also to enhance the operating temperature of the engine [1–5]. A typical TBC system includes MCrAlY (M = Co and/or Ni) metallic bondcoat as oxidation resistant layer and partially stabilized zirconia topcoat as thermal insulation layer. The metallic bondcoat is deposited between the metallic substrate and the ceramic topcoat to protect the underlying metal from oxidation and high temperature corrosion and to enhance the adherence between the dissimilar substrate and topcoat [6–9]. The topcoat is usually applied either by an air plasma spray (APS) or electron beam physical vapor deposition (EB-PVD) [10–12]. However, because the capital cost in setting up a commercial EB-PVD plant is high, plasma spray methods have found wide acceptance so far [13]. Plasma sprayed TBCs have also a low thermal conductivity combined with a good chemical stability at high temperature [14]. MCrAlY coatings can be produced by thermally spraying methods or physical vapor deposition (PVD) processes [15]. To create surface of high roughness and of development to get the best joint with ceramic topcoat, deposited by the APS method, the bondcoat is required to be deposited by the spraying methods [16].

Yttria stabilized zirconia (YSZ) has been usually chosen for the top insulating coat material because of its high coefficient of thermal expansion (CTE), which closely matches that of the substrate and low thermal conductivity [17–20]. However, severe operating conditions can reduce the performance of the state-of-the-art YSZ coatings [21]. YSZ based TBC systems in the presence of molten salts, such as Na, S and V, contained in low quality fuels, involve corrosion problems and cannot be successfully applied [22]. Vanadium and sodium are common impurities in low grade petroleum fuels. Molten sulfate–vanadate deposits resulting from the condensation of combustion products of such fuels are

*Corresponding author. Tel.: +98 312 5225041; fax: +98 312 5228530.
E-mail address: ra-ahmadi@mut-es.ac.ir (R. Ahmadi-Pidani).

0272-8842/$36.00
http://dx.doi.org/10.1016/j.ceramint.2012.05.047

extremely corrosive to high-temperature materials in combustion systems [23–26]. Much efforts have been devoted to improve the phase stability and hot corrosion resistance of the traditional YSZ material by doping new metal oxides such as In_2O_3, Sc_2O_3, CeO_2, etc [21,22,27].

Previous results [21,28] demonstrated that when applied in a more demanding environment, such as higher temperatures, corrosion and stress were scrutinized, the ZrO_2–Y_2O_3–CeO_2 (CYSZ) coating appeared to be promising. It has been indicated that the CYSZ coating was superior to the YSZ coating due to its phase stability at high temperature [21,28–30], improved thermal insulation, higher CTE [28], good corrosion and thermal shock resistance [21,28,29].

In many studies, hot corrosion behavior of YSZ coatings was evaluated frequently, but little attention has been paid to CYSZ coatings so far. Jones [22,31] summarized the results of a research effort aimed at identifying hot corrosion-resistant stabilizers for zirconia such as TiO_2, CeO_2, Y_2O_3, MgO, SC_2O_3, In_2O_3 and SnO_2 which could be used in zirconia-based TBCs for engines operating on marine fuel under seagoing conditions. He described hot corrosion mechanism of ceria stabilized zirconia (CSZ), but hot corrosion mechanism of CYSZ has not been clearly explained. Park et al. [32] compared the hot corrosion properties of YSZ and CYSZ TBCs under a $NaVO_3$ salt environment at 900 °C, but all occurred events were not described in detail. Therefore, detailed studies on corrosion resistance of CYSZ TBCs are required to methodically clarify the performance of these TBCs under corrosive conditions.

In this paper, a study with focus on hot corrosion response of CYSZ ceramic coatings, in the presence of $V_2O_5+Na_2SO_4$ molten salt, is reported. The mechanism of degradation of coatings is also suggested.

2. Materials and methods

2.1. Material

Inconel 738 LC superalloy was used as the substrate with the dimension of 16 mm × 16 mm × 10 mm. The spray powders were commercial NiCoCrAlY powder (22 SN 6883, S.N.M.I.-Avignon) and ZrO_2-25 wt%$CeO_2-2.5$ wt%Y_2O_3 (205NS, Sulzer Metco) and were deposited by air plasma spraying. Some specifications and SEM micrographs of powders are shown in Table 1 and Fig. 1, respectively.

2.2. Air plasma spraying

Plasma spraying was carried out with a Plasma Technik AG; Switzerland F4-MB gun (Sulzer-Metco; Switzerland) in air. Spraying parameters are shown in Table 2. In order to increase the surface roughness and promote coating adhesion, the substrates were grit blasted with alumina. The measured surface roughness (R_a) of substrates was 9.20 μm.

They were also degreased and cleaned with acetone and preheated with plasma gun prior to spraying. The sprayed

Table 2
Plasma spraying parameters.

Parameter	NiCoCrAlY	CYSZ
Voltage (V)	75	61
Current (A)	600	600
Primary gas, Ar (slmp)	65	35
Secondary gas, H_2 (slmp)	14	12
Carrier gas, Ar (slmp)	2.3	2.6
Powder feed rate (g/min)	40	40
Spray distance (mm)	120	120

Table 1
Spray powders specifications.

Type of powder	Particle size (μm)	Manufacturing method	Morphology
CYSZ	16–90	Agglomerated and plasma densified	Spheroidal, HOSP[a]
NiCoCrAlY	38–75	Gas atomized	Spheroidal

[a]Homogenous Oven Spherical Powder.

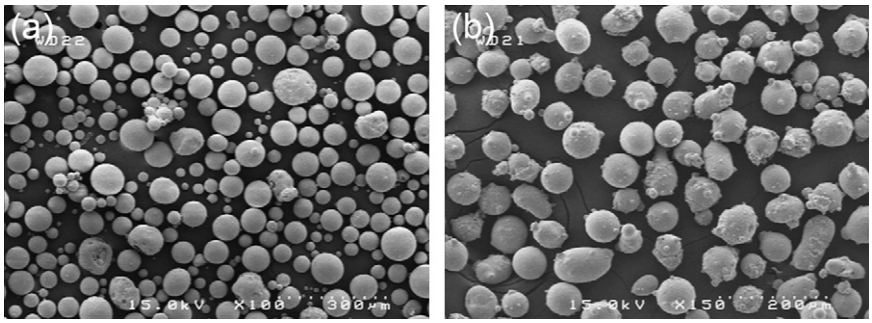

Fig. 1. FESEM micrographs of CYSZ (a) and NiCoCrAlY (b) spray powders.

Table 3
Corrosive salts specifications.

Type of salt	V_2O_5	Na_2SO_4
Manufacturer	Merck (Germany)	Merck (Germany)
Density (g/cm^3)	3.36	2.70
Melting point (°C)	690	888

coating was formed directly on the substrate and were cooled by air blowing onto the surface.

2.3. Hot corrosion test

In order to evaluate hot corrosion behavior of coatings, a mixture of 55 wt%V_2O_5 and 45 wt%Na_2SO_4 powders was selected as a corrosive salt. Some specifications of each salt are presented in Table 3. The corrosive powders were strewed over the surface of coatings in a 25 mg/cm^2 concentration leaving approximately 3 mm from the edge uncovered. The specimens were set in an electric furnace with air atmosphere at 1000 °C for 30 h and then, were left outside to let it cool down in the air. The specimens were inspected periodically every 6 h.

2.4. Characterization

The microstructure of coatings was evaluated using a field emission scanning electron microscope (FE-SEM) (S-4160, Hitachi Ltd., Japan). The elemental composition of corrosion products was investigated by energy dispersive spectroscopy (EDS) analysis. The phases were analyzed using X-Ray diffractometer (XRD) (Bruker-D8 ADVANCE, Germany) with filtered Cu Kα radiation (0.15406 nm). The surface roughness (R_a) of substrates prior to spraying was measured by a roughness tester (Mitutoyo SJ-201P, Japan).

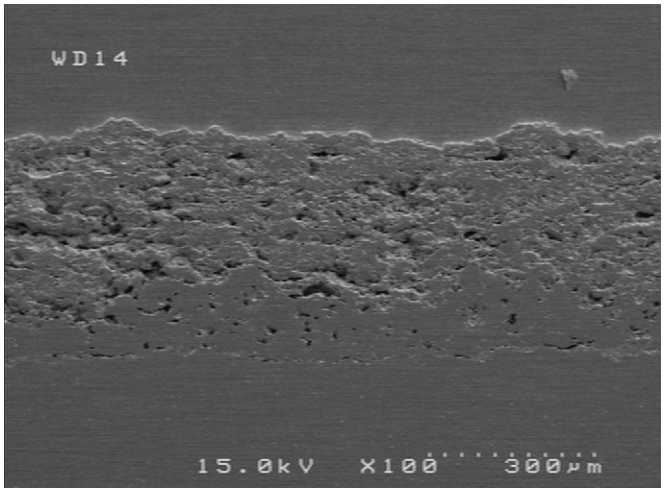

Fig. 2. FESEM micrograph of polished cross section of as sprayed CYSZ/NiCoCrAlY TBC system.

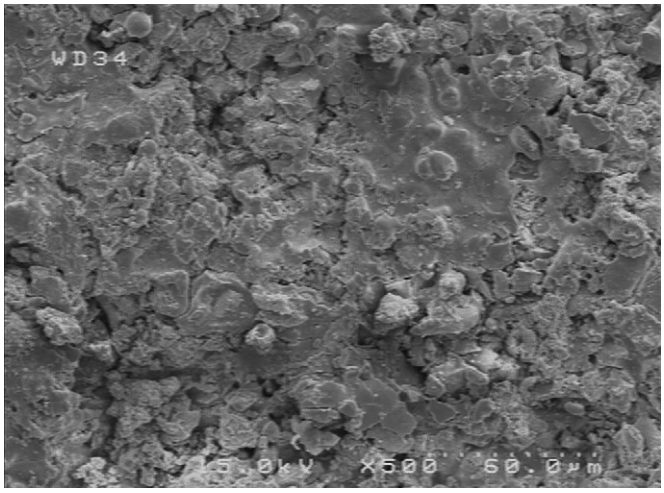

Fig. 3. FESEM micrograph of top surface of as sprayed CYSZ coating.

3. Result and discussion

3.1. Characterization of as sprayed coatings

Fig. 2 shows the polished cross section of the as sprayed thermal barrier coating system. In this figure, different layers of usual TBC can be observed which include NiCoCrAlY bondcoat and CYSZ topcoat. The image analysis results indicated that the porosity of CYSZ coating is 11.39%. Such value guarantees a good compromise in terms of low thermal conductivity [33].

Fig. 3 shows the FESEM micrograph of top surface of as sprayed CYSZ coating. As shown in Fig. 3, the top surface of coating is very rough because it includes of splats (molten particles deformed on impact into a pancake shape) that deposited on surface with different flattening parameters. Enclosing transverse microcracks, porosity and occasional unmelted particles are also visible. These defects are common properties of plasma sprayed ceramic coatings that play an important role in hot corrosion behavior of TBC systems as effective penetration paths of molten salts [32].

Fig. 4 presents the fractured cross section of plasma sprayed ceramic topcoat. As can be seen, the coating shows a layered structure including the splats that are placed on each other. In order to understand the formation of microstructure of plasma sprayed ceramic coating, we need to follow the sequence of events leading to a molten droplet depositing on the substrate and freezing to a solid. Plasma spray is a stochastic process in which a stream of molten particles strikes the surface of the work piece where they undergo rapid deformation and solidification to form disk-like splats [33]. In fact, molten particles continue depositing on previously piled up solidified splats and coating built as particle by particle with characteristic splat morphology [34,35]. As shown in Fig. 4, the structure within each splat is crystalline with well-defined columnar grains. The heights of the columns typically equal the thickness of the splats. This columnar structure has formed by directional solidification at rapid cooling [33]. Also, the

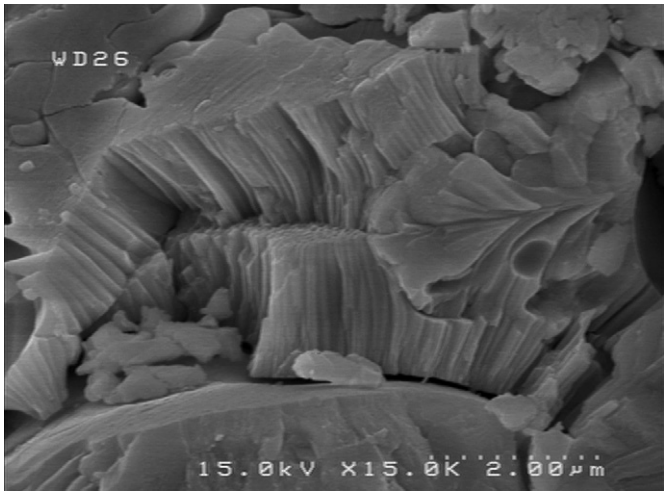

Fig. 4. FESEM micrograph of fractured cross section of as sprayed CYSZ coating.

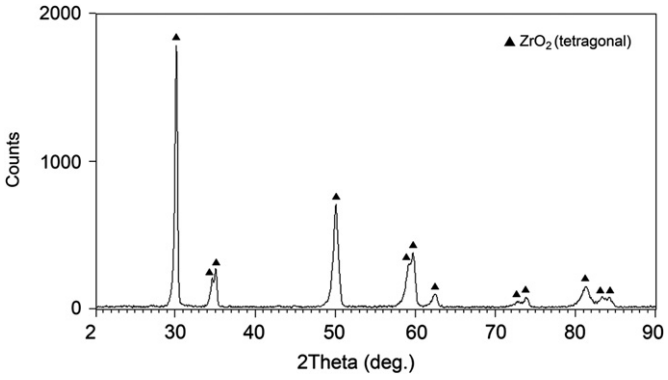

Fig. 5. XRD pattern of as sprayed CYSZ coating.

presence of intra-splat cracks in the splat structure is evident. The formation of these cracks is attributed to residual stresses during the deposition process [33,36]. The presence of inter-splat voids and pores can be dependent on random deposition [37], the lack of complete overlap of adjacent splats [38], and gas entrapment during the deposition process [36,39].

The XRD pattern of as sprayed coating is shown in Fig. 5. According to this pattern, CYSZ coating consisted of nontransformable tetragonal (t') phase. The t' phase is a kind of nonequilibrium phase formed due to the rapid solidification of molten particles [33]. The extremely high cooling rate ($\sim 10^6$ K/s) in the plasma sprayed particles prevents the harmful phase transformation of zirconia from the tetragonal to the monoclinic and creates the nontransformable tetragonal zirconia from the cubic phase by a martensitic phase transformation [35]. Therefore, presence of zirconia in the t' phase after plasma spraying is a common subject that other researchers also refer to [35,40,41].

3.2. Characterization of coatings after hot corrosion

Fig. 6 shows the FESEM micrographs of top surface of coatings after 6, 18, and 30 h hot corrosion. As clearly shown in this figure, the semi-cubic (B) and rod-type crystals (C) have been formed on the coating surface (A). The XRD patterns of coatings after 6, 18, and 30 h hot corrosion are shown in Fig. 7. According to these patterns, zirconia is present in tetragonal and monoclinic phases, while as sprayed coating was contained only in a tetragonal phase (Fig. 5). In addition, the formation of YVO_4,

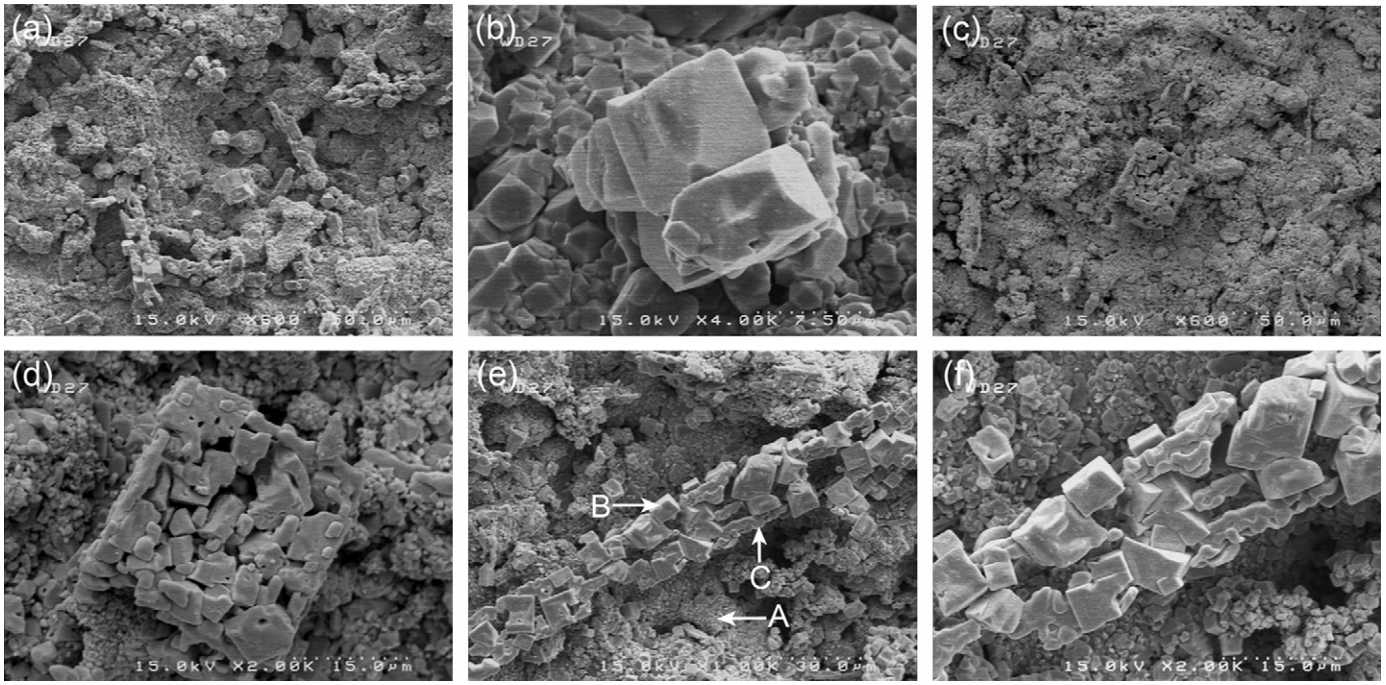

Fig. 6. FESEM micrographs of top surface of coatings after 6 h (a) and (b), 18 h (c) and (d), and 30 h (e) and (f) hot corrosion.

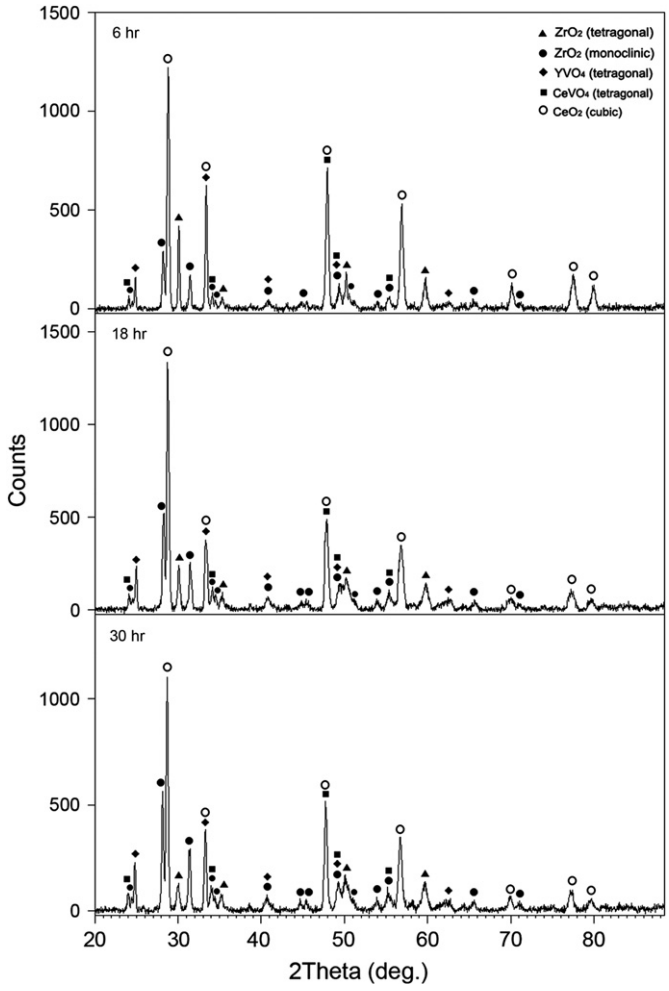

Fig. 7. XRD patterns of coatings after 6, 18, and 30 h hot corrosion.

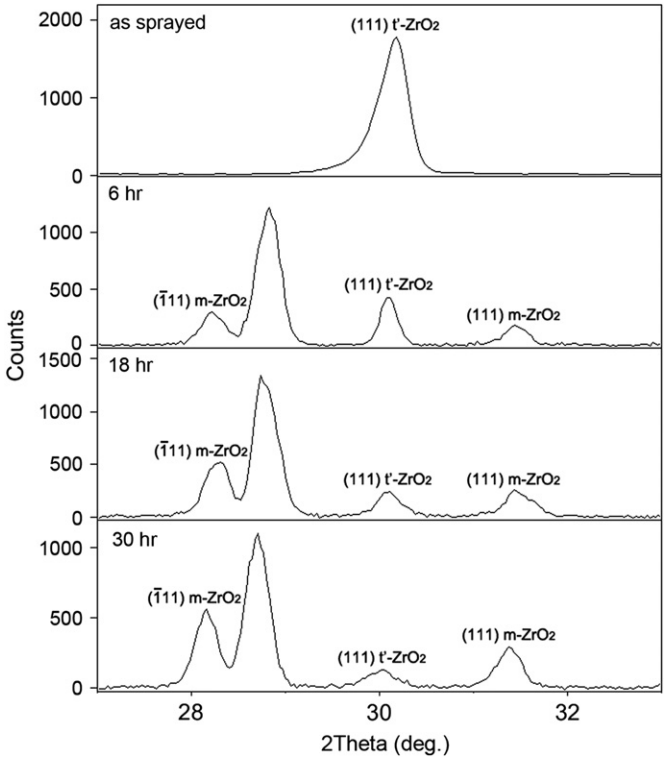

Fig. 8. XRD patterns of coatings before and after 6, 18, and 30 h hot corrosion.

Table 4
Volume fractions of m-ZrO_2 (%m) during hot corrosion test.

Corrosion time (hr)	0	6	18	30
m-ZrO_2 (%)	0	52.1	76.4	86.0

$CeVO_4$, and CeO_2 on the surface, during the hot corrosion test, is demonstrated.

A region of XRD pattern, with the mean peak of tetragonal and monoclinic phases (27°–32°), is shown in Fig. 8. As can be seen, there was no monoclinic phase in coating before hot corrosion (Fig. 8a), but during hot corrosion test, the mean peaks of monoclinic phases ($m(\bar{1}11)$ and $m(111)$) appeared, and their relative intensities were increased at time lapse, and the relative intensity of the tetragonal mean peak ($t(111)$) was decreased (Fig. 8b–d). The volume fractions of m-ZrO_2 (%m), as the criteria for coatings destabilization during hot corrosion test, are compared in Table 4, which were calculated by the peak intensity ratio formula [40,42,43]:

$$\%m = \frac{I_m(\bar{1}11)+I_m(111)}{I_m(\bar{1}11)+I_m(111)+I_t(111)} \times 100 \quad (1)$$

where, I represent the diffraction intensity of the respective lattice planes. According to Eq. (1), the volume fraction of m-ZrO_2 was increased to 86%, as corrosion time was increased.

The EDS analysis of A, B and C points shows that the coating surface "A" contains Zr, Ce, Y and O (Fig. 9a), the semi-cubic crystals "B"; contain Ce and O (Fig. 9b), and the rod-type crystals "C" contain Ce, Y, V and O elements (Fig. 9c). Therefore, according to FESEM micrographs, EDS and XRD patterns, it is demonstrated that the coating surface "A" is ceria and yttria stabilized zirconia, semi-cubic crystals "B" were CeO_2 and rod-type crystals "C" were mixture of YVO_4 and $CeVO_4$.

3.3. Description of reactions

In order to understand hot corrosion mechanism of CYSZ coatings, in the presence of sulfate–vanadate molten salts, we need to follow the sequence of reactions leading to the production of above crystals and degradation of coating.

The reaction of salts, together and with coating stabilizer, can be described as follows:

At first, $NaVO_3$ was formed after the reaction of initial salts (mixture of sodium sulfate and vanadium oxide) at high temperature by the following reactions [22,31]:

$$Na_2SO_4\ (l) \rightarrow Na_2O\ (l) + SO_3\ (g)$$

$$Na_2O\ (l) + V_2O_5\ (l) \rightarrow 2NaVO_3(l)$$

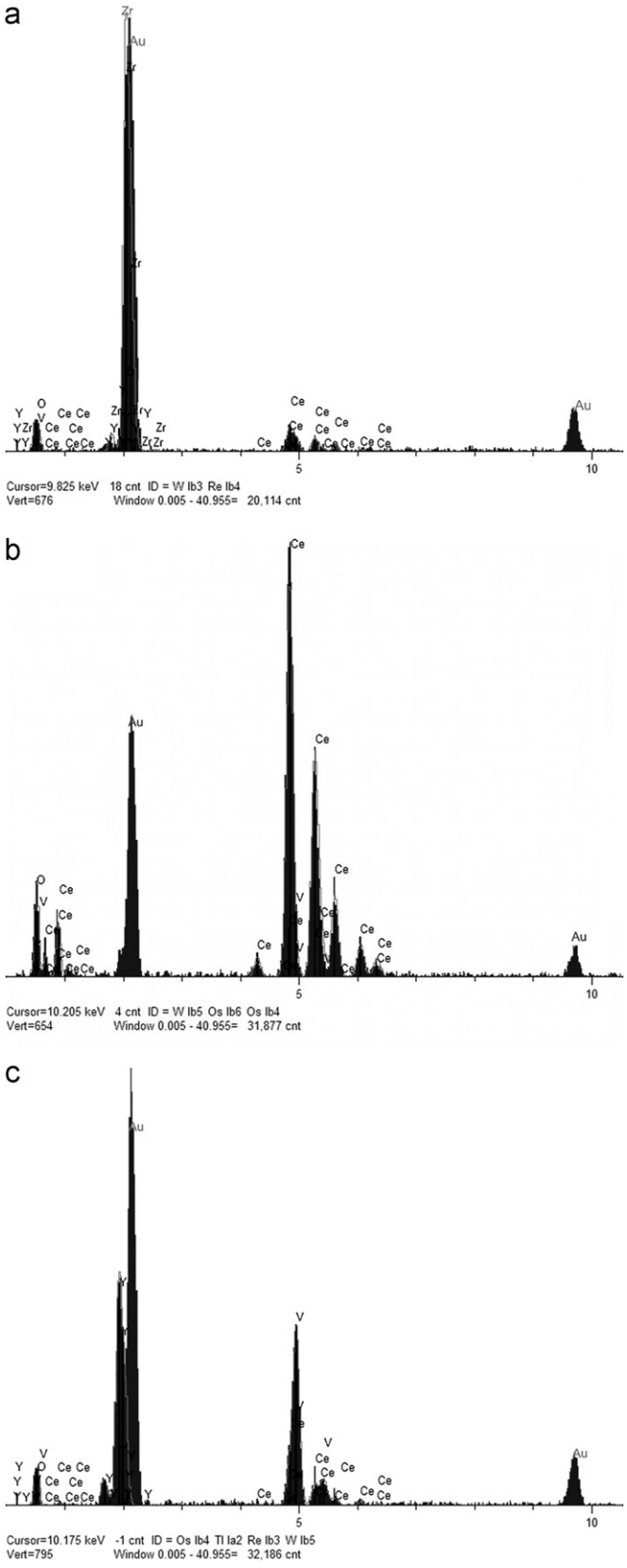

Fig. 9. EDS analysis of A (a), B (b), and C (c) points as shown in Fig. 5.

The molten $NaVO_3$ can easily penetrate to the coating through the open pores and microcracks that exist on the surface due to plasma spraying process [32]. Penetrated $NaVO_3$ reacts with Y_2O_3 to produce monoclinic ZrO_2, YVO_4 and Na_2O:

$$ZrO_2 \cdot Y_2O_3\ (s) + 2NaVO_3\ (l) \rightarrow m\text{-}ZrO_2\ (s) + 2YVO_4\ (s) + Na_2O\ (l)$$

In EDS analysis performed on different points of coating surface, Na was not detected. It seems that Na_2O is sublimated during hot corrosion tests, considering that this result was confirmed by other researchers [44].

Different studies [45,46], with regard to YSZ hot corrosion, reported that Y_2O_3 reacted with the V_2O_5 to form YVO_4 by the following reaction:

$$ZrO_2 \cdot Y_2O_3\ (s) + V_2O_5\ (l) \rightarrow m\text{-}ZrO_2\ (s) + 2YVO_4\ (s)$$

Laboratory tests with regard to Lewis acid–base lows indicate that molten $NaVO_3$ does not react with CeO_2 [44]. Despite this fact, Park et al. [32] demonstrated that both the free CeO_2 precipitates and CeO_2 stabilizers remaining in zirconia reacted with the $NaVO_3$ salts to form $CeVO_4$.

Other laboratory tests indicated that CSZ was destabilized by molten $NaVO_3$, even though pure ZrO_2 and CeO_2 separately did not react chemically with $NaVO_3$. The product of destabilization was monoclinic ZrO_2 with surface crystals of CeO_2, were in fact the equilibrium phases for the ZrO_2–CeO_2 system at 700–900 °C. The destabilization of CSZ by pure molten $NaVO_3$ is, therefore, evidently a mineralization effect. In contrast, when CSZ is destabilized by V_2O_5 or $NaVO_3$–V_2O_5 mixtures, the reaction product, $CeVO_4$, is found, indicating that destabilization in this case is occurred by chemical reaction [22,31]. Park et al. [32] also agreed that the formation of free ceria on the CSZ surface was due to "mineralization".

No evidence from XRD patterns was found to show that the chemical reaction between Na_2SO_4 and CYSZ had taken place. This indicates that Na_2SO_4 had no chemical effect on CYSZ coating at this temperature. Zhong et al. [40] also confirmed that Na_2SO_4 had no chemical effect on YSZ coating at the elevated temperature of 1000 °C.

Another possible chemical reaction would be the zirconia matrix itself with the molten vanadate:

$$ZrO_2 + V_2O_5 \rightarrow ZrV_2O_7$$

However, XRD analysis also showed that any reaction product of V_2O_5 with ZrO_2 could not be detected after hot corrosion tests. This result is in conformity with literatures that mentions the reaction kinetics is slow and not usually detected [40,42,46]. It is known that zirconium pyrovanadate (ZrV_2O_7) is the only compound existing in the ZrO_2–V_2O_5 system. ZrV_2O_7 melts at a temperature above 1020 K to ZrO_2 and V_2O_5 [40] and therefore, no reaction product of V_2O_5 with ZrO_2 was found in this investigation.

3.4. Determination of hot corrosion mechanism of CYSZ coatings

As mentioned earlier, the plasma sprayed CYSZ coating had various defects, such as microcracks, inter splat voids

and open pores (Fig. 4). Therefore, molten salts can penetrate in the coating from these effective penetration paths. According to the possible reactions, chemical degradation was initiated in the interface of molten salt and CYSZ splats by nucleation and growth of YVO_4 and $CeVO_4$ in the shape of rod-type crystals. In addition, CeO_2 was mineralized into semi-cubic crystals. These crystals grow outward of the surface (Fig. 6) and can lead to additional stresses in the coating [44].

The t' phase of CYSZ is stabilized by the presence of CeO_2 and Y_2O_3 stabilizers. With reactions progression, depletion of ceria and yttria stabilizers from zirconia structure results in phase transformation from t'- to m-ZrO_2. The process of t'- to m-ZrO_2 transformation is a diffusionless, martensitic-type which is accompanied by a large destructive volume expansion [40,43]. The volume expansion stresses can lead to cracks in the coating upon cooling and may cause coating failure.

The cross section micrograph of the coating after hot corrosion test is shown in Fig. 10. It is clearly shown in Fig. 10 that cracking occurred in the topcoat. The creation of these cracks can be related to the stresses resulting from formation of the monoclinic ZrO_2 and YVO_4, $CeVO_4$, and CeO_2 crystals. Based on Fig. 10, a black thin layer between the ceramic topcoat and bondcoat is also observed. This thin layer which is called as the thermally grown oxide (TGO) is formed due to transfer of oxygen through the topcoat towards the bondcoat and oxidation of bondcoat [24,43,47]. With further exposure of coating to high temperature, thickening of this layer may contribute to TBCs failure [18,33,48].

Therefore, hot corrosion behavior and failure mechanism of CYSZ TBCs in the present study involve the following steps that are in agreement with Jones [22,31] investigations:

(1) Penetration of molten salts through coating microcracks and open pores.

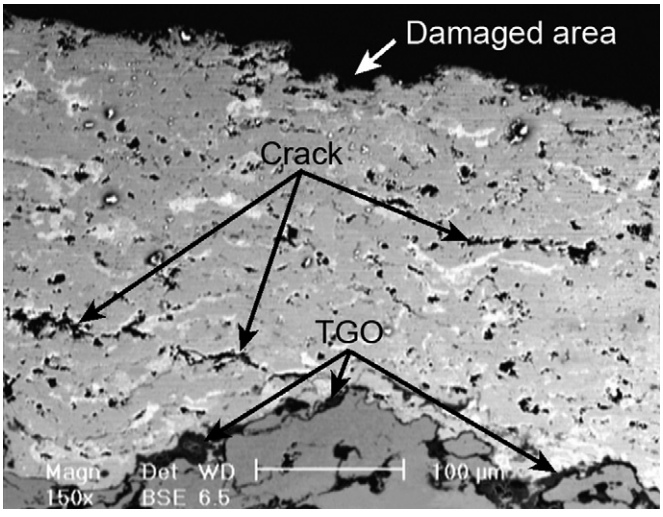

Fig. 10. SEM Micrograph of cross section of coating after 30 h hot corrosion.

(2) Interaction of molten salts with zirconia stabilizers (Y_2O_3 and CeO_2):
   (a) Chemical reaction of salts with stabilizers to form YVO_4 and $CeVO_4$ rod-type crystals.
   (b) Mineralization of CeO_2 as the semi-cubic crystals.
(3) The t'- to m-ZrO_2 transformation due to stabilizers depletion which is accompanied by a large destructive volume expansion.
(4) Creation of cracks in the ceramic coating due to the stresses resulting from formation of the monoclinic ZrO_2 and YVO_4, $CeVO_4$, and CeO_2 crystals, and bondcoat oxidation that can lead to coating failure.

4. Conclusion

The NiCoCrAlY/CYSZ thermal barrier coatings on IN738 LC superalloy were prepared by air plasma spraying. Hot corrosion behavior of coatings in the presence of $Na_2SO_4+V_2O_5$ molten salt at 1000 °C for 30 h was evaluated. According to microscopic observation, XRD analysis and EDS analysis results, a possible degradation mechanism of hot corrosion in CYSZ coatings was discussed. Based on this, molten salts were penetrated through coating microcracks and open pores and interacted with zirconia stabilizers (Y_2O_3 and CeO_2) to form YVO_4 and $CeVO_4$ rod-type crystals and CeO_2 semi-cubic crystals. With reactions progression, the depletion of stabilizers from zirconia structure occurred and resulted in phase transformation from t'- to m-ZrO_2. This transformation is accompanied by a large destructive volume expansion. Finally, the stresses resulting from formation of the monoclinic ZrO_2 and YVO_4, $CeVO_4$, and CeO_2 crystals and bondcoat oxidation can lead to crack formation and failure of TBC.

References

[1] S. Das, S. Datta, D. Basu, G.C. Das, Thermal cyclic behavior of glass–ceramic bonded thermal barrier coating on nimonic alloy substrate, Ceramics International 35 (2009) 2123–2129.
[2] C.S. Ramachandran, V. Balasubramanian, P.V. Ananthapadmanabhan, V. Viswabaskaran, Influence of the intermixed interfacial layers on the thermal cycling behaviour of atmospheric plasma sprayed lanthanum zirconate based coatings, Ceramics International (2012)http://dx.doi.org/10.1016/j.ceramint.2012.01.066.
[3] C.K. Roy, M. Noor-A-Alam, A.R. Choudhuri, C.V. Raman, Synthesis and microstructure of Gd_2O_3-doped HfO_2 ceramics, Ceramics International 38 (2012) 1801–1806.
[4] L. Wang, Y. Wang, X.G. Sun, J.Q. He, Z.Y. Pan, C.H. Wang, Thermal shock behavior of 8YSZ and double-ceramic-layer $La2Zr_2O_7$/8YSZ thermal barrier coatings fabricated by atmospheric plasma spraying, Ceramics International (2012)http://dx.doi.org/10.1016/j.ceramint.2011.12.076.
[5] Q. Yu, A. Rauf, Na. Wang, C. Zhou, Thermal properties of plasma-sprayed thermal barrier coating, with bimodal structure, Ceramics International 37 (2011) 1093–1099.
[6] S. Das, S. Datta, D. Basu, G.C. Das, Glass–ceramics as oxidation resistant bond coat in thermal barrier coating system, Ceramics International 35 (2009) 1403–1406.
[7] Y. Li, Y. Xie, L. Huang, X. Liu, X. Zheng, Effect of physical vapor deposited Al_2O_3 film on TGO growth in YSZ/CoNiCrAlY coatings,

Ceramics International (2012)http://dx.doi.org/10.1016/j.ceramint.2012.03.014.
[8] R. Vaßen, M.O. Jarligo, T. Steinke, D.E. Mack, D. Stöver, Overview on advanced thermal barrier coatings, Surface and Coatings Technology 205 (2010) 938–942.
[9] M. Alfano, G. Di Girolamo, L. Pagnotta, D. Sun, Processing, microstructure and mechanical properties of air plasma-sprayed ceria–yttria co-stabilized zirconia coatings, Strain 46 (2010) 409–418.
[10] J. Fenech, C. Viazzi, J. Bonino, F. Ansart, A. Barnabe, Morphology and structure of YSZ powders: comparison between xerogel and aerogel, Ceramics International 35 (2009) 3427–3433.
[11] R.W. Steinbrech, V. Postolenko, J. Monch, J. Malzbender, L. Singheiser, Testing method to assess lifetime of EB-PVD thermal barrier coatings on tubular specimens in static and cyclic oxidation tests, Ceramics International 37 (2011) 363–368.
[12] S. Guo, Y. Kagawa, Effect of thermal exposure on hardness and Young's modulus of EB-PVD yttria-partially-stabilized zirconia thermal barrier coatings, Ceramics International 32 (2006) 263–270.
[13] R. Ahmadi-Pidani, R. Shoja-Razavi, R. Mozafarinia, H. Jamali, Improving the thermal shock resistance of plasma sprayed CYSZ thermal barrier coatings by laser surface modification, Optics and Lasers in Engineering 50 (2012) 780–786.
[14] X. Ma, S. Cho, M. Takemoto, Acoustic emission source analysis of plasma sprayed thermal barrier coatings during four-point bend tests, Surface and Coatings Technology 139 (2001) 55–62.
[15] H.E. Evans, High temperature coatings: protection and breakdown, in: T. Richardson, B. Cottis, R. Lindsay, S. Lyon, D. Scantlebury (Eds.), Shreir's Corrosion, Elsevier, Manchester, 2010, pp. 691–724.
[16] G. Moskal, Thermal barrier coatings: Part 1—characteristics of microstructure and properties, generation and directions of development of bond, Archives of Materials Science 28 (2007) 100–112.
[17] R. Ahmadi-Pidani, R. Shoja-Razavi, R. Mozafarinia, H. Jamali, Comparison of hot corrosion resistance of YSZ and CYSZ thermal barrier coatings in presence of sulfate–vanadate molten salts, Advances in Materials Research 472–475 (2012) 141–144.
[18] H. Jamali, R. Mozafarinia, R. Shoja-Razavi, R. Ahmadi-Pidani, Investigation of thermal shock behavior of plasma-sprayed NiCoCrAlY/YSZ thermal barrier coatings, Advances in Materials Research 472–475 (2012) 246–250.
[19] N. Wang, C. Zhou, S. Gong, H. Xu, Heat treatment of nanostructured thermal barrier coating, Ceramics International 33 (2007) 1075–1081.
[20] W.B. Gong, C.K. Sha, D.Q. Sun, W.Q. Wang, Microstructures and thermal insulation capability of plasma-sprayed nanostructured ceria stabilized zirconia coatings, Surface and Coatings Technology 201 (2006) 3109–3115.
[21] G.D. Girolamo, C. Blasi, M. Schioppa, L. Tapfer, Structure and thermal properties of heat treated plasma sprayed ceria–yttria co-stabilized zirconia coatings, Ceramics International 36 (2010) 961–968.
[22] R.L. Jones, Some aspects of the hot corrosion of thermal barrier coatings, Journal of Thermal Spray Technology 6 (I) (1997) 77–84.
[23] T.S Sidhu, R.D. Agrawal, S. Prakash, Hot corrosion of some superalloys and role of high-velocity oxy-fuel spray coatings—a review, Surface and Coatings Technology 198 (2005) 441–446.
[24] M. Saremi, A. Afrasiabi, A. Kobayashi, Bond coat oxidation and hot corrosion behavior of plasma sprayed YSZ coting on Ni superalloy, Transactions of JWRI 36 (2007) 41–45.
[25] H. Huang, C. Liu, L. Ni, C. Zhou, Evaluation of microstructural evolution of thermal barrier coatings exposed to Na_2SO_4 using impedance spectroscopy, Corrosion Science 53 (2011) 1369–1374.
[26] S. Li, Z.G. Liu, J.H. Ouyang, Hot corrosion behaviour of $Yb_2Zr_2O_7$ ceramic coated with V_2O_5 at temperatures of 600–800 °C in air, Corrosion Science 52 (2010) 3568–3572.
[27] X. Chen, Y. Zhao, L. Gu, B. Zou, Y. Wang, X. Cao, Hot corrosion behaviour of plasma sprayed YSZ/$LaMgAl_{11}O_{19}$ composite coatings in molten sulfate–vanadate salt, Corrosion Science 53 (2011) 2335–2343.
[28] J.H. Lee, P.C. Tsai, C.L. Chang, Microstructure and thermal cyclic performance of laser-glazed plasma-sprayed ceria–yttria-stabilized zirconia thermal barrier coatings, Surface and Coatings Technology 202 (2008) 5607–5612.
[29] P. Ramaswamy, S. Seetharamu, K.B.R. Varma, K.J. Rao, Evaluation of CaO–CeO_2-partially stabilized zirconia thermal barrier coatings, Ceramics International 25 (1999) 317–324.
[30] H. Choi, H. Kim, C. Lee, Phase evolutions of plasma sprayed ceria and yttria stabilized zirconia thermal barrier coating, Journal of Materials Science Letters 21 (2002) 1359–1361.
[31] R.L. Jones, Experiences in Seeking Stabilizers for Zirconia Having Hot Corrosion-Resistance and High Temperature Tetragonal (t') Stability, Naval Research Laboratory, Washington, 1996.
[32] S.Y. Park, J.H. Kim, M.C. Kim, H.S. Song, C.G. Park, Microscopic observation of degradation behavior in yttria and ceria stabilized zirconia thermal barrier coatings under hot corrosion, Surface and Coatings Technology 190 (2005) 357–365.
[33] S. Bose, High Temperature Coatings, Elsevier Science & Technology Books, Connecticut, USA, 2007.
[34] R.C. Reed, The Superalloys: Fundamentals and Applications, Cambridge University Press, UK, 2006.
[35] H. Jamali, R. Mozafarinia, R. Shoja-Razavi, R. Ahmadi-Pidani, M.R. Loghman-Estarki, Fabrication and evaluation of plasma-sprayed nanostructured and conventional YSZ thermal barrier coatings, Current Nanoscience 8 (2012) 402–409.
[36] O. Racek, C.C. Berndt, D.N. Guru, J. Heberlein, Nanostructured and conventional YSZ coatings deposited using APS and TTPR techniques, Surface and Coatings Technology 201 (2006) 338–346.
[37] R.S. Lima, A. Kucuk, C.C. Berndt, Integrity of nanostructured partially stabilized zirconia after plasma spray processing, Materials Science and Engineering A 313 (2001) 75–82.
[38] L. Wang, Y. Wang, X.G. Sun, J.Q. He, Z.Y. Pan, Y. Zhou, P.L. Wu, Influence of pores on the thermal insulation behavior of thermal barrier coatings prepared by atmospheric plasma spray, Materials and Design 32 (2011) 36–47.
[39] O. Racek, C.C. Berndt, Mechanical property variations within thermal barrier coatings, Surface and Coatings Technology 202 (2007) 362–369.
[40] X.H. Zhong, Y.M. Wang, Z.H. Xu, Y.F. Zhang, J.F. Zhang, X.Q. Cao, Hot-corrosion behaviors of overlay-clad yttria-stabilized zirconia coatings in contact with vanadate–sulfate salts, Journal of the European Ceramic Society 30 (2010) 1401–1408.
[41] D.W. Parker, Thermal barrier coatings for gas turbines, automotive engines and diesel equipment, Materials and Design 13/6 (1992) 345–351.
[42] C. Batista, A. Portinha, R.M. Ribeiro, V. Teixeira, C.R. Oliveira, Evaluation of laser-glazed plasma-sprayed thermal barrier coatings under high temperature exposure to molten salts, Surface and Coatings Technology 200 (2006) 6783–6791.
[43] Z. Xu, L. He, R. Mu, S. He, G. Huang, X. Cao, Hot corrosion behavior of rare earth zirconates and yttria partially stabilized zirconia thermal barrier coatings, Surface and Coatings Technology 204 (2010) 3652–3661.
[44] A. Afrasiabi, M. Saremi, A. Kobayashi, A comparative study on hot corrosion resistance of three types of thermal barrier coatings: YSZ, YSZ + Al_2O_3 and YSZ/Al_2O_3, Materials Science and Engineering A 478 (2008) 264–269.
[45] H.G. Rubahn, Laser Applications in Surface Science and Technology, John Wiley and Sons, New York, 1999.
[46] I. Gurrappa, Thermal barrier coatings for hot corrosion resistance of CM 247 LC superalloy, Journal of Materials Science Letters 17 (1998) 1267–1269.
[47] D. Seo, K. Ogawa, Y. Nakao, H. Miura, T. Shoji, Influence of high-temperature creep stress on growth of thermally grown oxide in thermal barrier coatings, Surface and Coatings Technology 203 (2009) 1979–1983.
[48] M.F. Morks, C.C. Berndt, Y. Durandet, M. Brandt, J. Wang, Microscopic observation of laser glazed yttria-stabilized zirconia coatings, Applied Surface Science 256 (2010) 6213–6218.